An Objective Climatology of Tropical Plumes

LUISE FRÖHLICH

Institute of Geophysics and Meteorology, University of Cologne, Cologne, Germany

PETER KNIPPERTZ

School of Earth and Environment, University of Leeds, Leeds, United Kingdom

ANDREAS H. FINK

Institute of Geophysics and Meteorology, University of Cologne, Cologne, Germany

ESTHER HOHBERGER

Institute of Flight Systems and Automatic Control, Technical University Darmstadt, Darmstadt, Germany

ABSTRACT

The first global objective climatology of tropical plumes (TPs), obtained from a novel algorithm based on gridded 10.8-μm brightness temperatures T_b, is presented for 1983–2006. TPs are defined as continuous cloud bands (>2000 km) crossing 15°N or 15°S with T_b anomalies of less than −20 K and a lifetime of at least 3 h. A minimum length-to-width ratio of 3 filters out elongated features. Numbers of identified TPs are sensitive to the chosen thresholds but not their geographical distribution and seasonal cycle.

TPs are an important indicator of tropical–extratropical interactions with impacts on radiation and moisture. TP occurrence during boreal winter is largely confined to oceanic regions with main maxima over the South Pacific and South Atlantic as well as the eastern North Atlantic and Pacific Oceans. The geographical distribution during boreal summer is similar, but with lower frequencies, except for monsoon-influenced regions. Interannual variations over the Indo-Pacific region are strongly related to El Niño. TPs often develop downstream of extratropical upper-level troughs propagating into low latitudes, particularly over the wintertime eastern North Pacific and North Atlantic, but also in regions where mean upper-level easterlies do not generally favor equatorward Rossby wave propagation. Synoptic-scale variations in the quasi-permanent cloud bands associated with the South Pacific and South Atlantic convergence zones frequently produce TP-like anomalies, which are climatologically associated with downstream upper-level troughs. Some regions also feature TPs associated with mesoscale tropical disturbances. The new TP algorithm will serve as a basis for more in-depth studies in the future.

1. Introduction

Interactions between the tropics and extratropics occur over a wide spectrum of processes and associated scales. Examples include synoptic- to planetary-scale Rossby wave trains connecting high and low latitudes, tropical-to-subtropical quasi-permanent low-level convergence zones, the intrusion of individual upper-level troughs into the tropics, and the recurvature of tropical cyclones into the extratropical westerlies. Often these interactions are visible on infrared (IR) satellite imagery through elongated diagonal cloud bands stretching from the tropics into the subtropics. Through their large extension in regions that are otherwise often cloud free, these bands affect the local and global radiation budget, mainly through enhanced reflection of solar radiation and absorption of thermal radiation (see case study in Knippertz and Fink 2008).

Quasi-permanent and quasi-stationary cloud bands form in relation to the South Pacific convergence zone (SPCZ; Kodama 1992, 1993; Vincent 1994), the South

Corresponding author address: Luise Fröhlich, Institut of Geophysics and Meteorology, University of Cologne, Kerpener Str. 13, 50937 Köln, Germany.
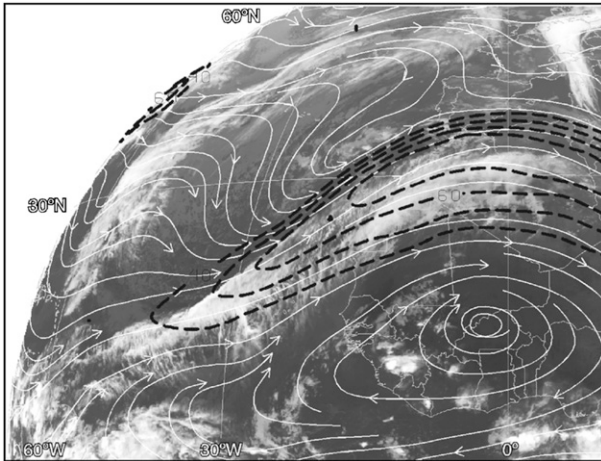E-mail: froehlil@uni-koeln.de

FIG. 1. Meteosat IR image of a TP over northwest Africa and the adjacent Atlantic Ocean at 0000 UTC 31 Mar 2002. Superimposed are streamlines and isotachs on the 345-K isentropic level (dashed contours at 40, 50, 60, and 70 m s^{-1}) from the ECMWF TOGA analysis (Fig. 1 from Knippertz 2007).

Atlantic convergence zone (SACZ; Carvalho et al. 2004), and the South Indian convergence zone (SICZ; Cook 2000), though the latter is less pronounced and restricted to austral summer. Over the western (North) Pacific, diagonal cloud bands often develop in association with upper-level outflow from nonrecurving tropical cyclones or extratropical transition and related frontogenesis of recurving tropical cyclones (Erickson and Winston 1972; Schnadt et al. 1998). Transient and short-lived diagonal cloud bands in relation to upper-level troughs are frequent over the North Atlantic and Pacific regions in boreal winter (Iskenderian 1995; Knippertz 2007). These elongated bands often consist of upper and midlevel clouds and can extend from the tropics over thousands of kilometers poleward and eastward into the subtropics or even midlatitudes (McGuirk et al. 1987; Knippertz 2005). They indicate momentum and moisture transports into higher latitudes and might be related to "atmospheric rivers" in some cases (Zhu and Newell 1998; Ralph et al. 2004, 2011). The poleward moisture transport occasionally leads to extreme precipitation events in the outer tropics or subtropics (Yoneyama and Parsons 1999; Fink and Knippertz 2003; Knippertz and Martin 2005, 2007). The IR satellite image from 0000 UTC 31 March 2002 shows an example over northwest Africa (Fig. 1), which was associated with an extreme rainfall event in southern Morocco and western Algeria (Fink and Knippertz 2003). McGuirk et al. (1988) were the first to coin the term "tropical plumes" (TPs) specifically for the diagonal cloud bands over the eastern North Pacific. Here, the term

will be used in a more general, global sense for all types of elongated cloud bands connecting the tropics and subtropics at synoptic time and spatial scales.

The advent of meteorological satellites in the 1970s enabled comprehensive observations and detailed descriptions of TPs. Several climatological TP studies in the past, all based on visual inspection of IR satellite imagery, gave insight into the geographical and seasonal variability of TP activity (McGuirk et al. 1987; Kuhnel 1989; Kodama 1993; Iskenderian 1995). Iskenderian (1995) constructed a composite of the 200-hPa streamfunction anomalies for 41 TPs over the tropical North Pacific. The anomaly pattern displays a wave train extending across the North Pacific and through the TP origin region with a northwest to southeast orientation. The propagation of such waves from the extratropics is usually described by linear Rossby wave theory (Hoskins and Ambrizzi 1993), which requires mean westerly background flow for the penetration of stationary Rossby wave disturbances into the tropics. Regions of upper-level equatorial westerlies, referred to as "westerly ducts" by Webster and Holton (1982), are observed during the boreal cool season over the equatorial eastern Pacific and Atlantic Oceans and are characterized by frequent incursions of upper extratropical troughs into low latitudes (Waugh and Polvani 2000; Fröhlich and Knippertz 2008).

To the best of our knowledge, the present study presents the first ever fully objective algorithm for the detection and tracking of TPs, which allows a flexible and quick processing of large datasets. By applying the new procedure to the brightness temperature T_b dataset from the Cloud Archive User Service (CLAUS) for the time period July 1983–June 2006, a 23-yr climatology is constructed and analyzed in detail. The remainder of the paper is structured as follows: A description of the dataset and the methodology is provided in section 2 together with an illustrative example. Geographical and seasonal distributions of TP activity are presented in section 3 together with an analysis of the robustness of the results. TP characteristics such as lifetime and horizontal tilt are statistically evaluated in section 4, while section 5 focuses on trends and interannual variability and the association with the El Niño–Southern Oscillation (ENSO). Based on composite studies, circulation anomalies in the upper troposphere in relation to TP occurrence are evaluated in section 6 to better understand the involved mechanisms. Section 7 discusses impacts of TPs on radiation and moisture distributions. In section 8, results are summarized and discussed and open questions for future research are presented.

2. Data and identification algorithm

a. Data

The main data used for the TP detection are T_b values from CLAUS, which are based on 10.8-μm thermal IR radiances (Hodges et al. 2000) measured by geostationary and polar-orbiting satellites participating in the International Satellite Cloud Climatology Project (ISCCP). The irregularly spaced source data were processed to give T_b values on a uniform latitude–longitude grid at a spacing of $0.5°$ every 3 h for the period from July 1983 to June 2006. Cold cloud tops are characterized by low T_b values, making it an appropriate parameter to separate cloudy from clear-sky areas. A limitation of these data is that information about the cloud distribution below the cloud top cannot be obtained.

To test the robustness of the TP identification algorithm it is also applied to the T_b dataset from the Pathfinder Atmospheres Extended (PATMOS-x) project (information available online at http://cimss.ssec.wisc.edu/patmosx/). The PATMOS-x dataset is derived directly from radiances measured by the polar-orbiting Advanced Very High Resolution Radiometer (AVHRR) instruments from 1981 to the present. In this work, the level-2b data product is employed that provides once-daily (estimated from the afternoon ascending orbits) fields of 11-μm brightness temperature on a $0.2°$ by $0.2°$ equal-area grid between $60°N$ and $60°S$.

All investigations on atmospheric circulation aspects are based upon the 40-yr European Centre for Medium-Range Weather Forecasts (ECMWF) Re-Analysis (ERA-40) dataset (Uppala et al. 2005). This dataset describes the state of the atmosphere every 6 h at a spectral resolution of T159L60 from December 1957 to February 2002. In this study, vertically averaged (100–400 hPa) potential vorticity (PV; as in Fröhlich and Knippertz 2008) and zonal winds, interpolated onto a $1° \times 1°$ latitude–longitude grid, are examined to analyze upper-level circulation anomalies in relation to TP occurrence. For background climatologies, the satellite era (1980–2001) of ERA-40 is used. The direct comparison with CLAUS data (as in Figs. 12, 13 in sections 6 and 7) is restricted to 1983–2001, for which both datasets are available.

To analyze interannual fluctuations in the TP time series in association with the ENSO phenomenon in section 5, the Niño-3.4 index from the Climate Prediction Center (CPC; http://www.cpc.ncep.noaa.gov/data/indices/) is used. Based on the Niño-3.4 index, six El Niño and five La Niña winter seasons are defined within the investigation period following Trenberth (1997), which are used to compile ENSO composites. In
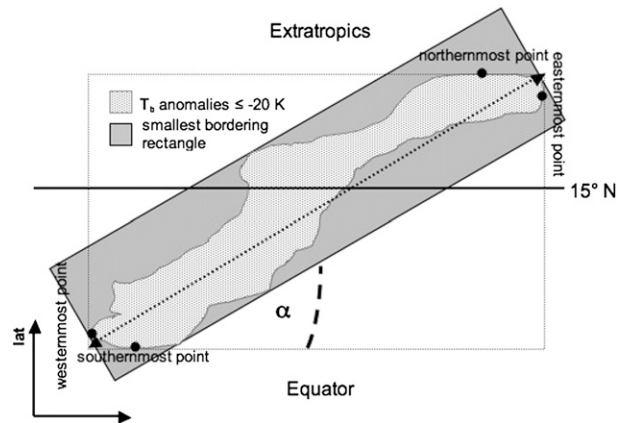

FIG. 2. Schematic illustration of the TP identification procedure for the NH. For more details, see section 2b.

addition, monthly indices of the North Atlantic Oscillation (NAO) and the Pacific/North American pattern (PNA), also taken from the CPC, were related to the TP climatology.

b. Identification algorithm

The objective algorithm for the identification of TPs proposed here largely follows the definition of McGuirk et al. (1987), who use the term ''moisture burst'' instead of TP. The identification routine uses T_b anomalies calculated from long-term monthly means. TP events are defined as contiguous regions with T_b anomalies $\leq$ -20 K of maximum extension ≥ 2000 km that cross $15°N$ in the Northern Hemisphere (NH) or $15°S$ in the Southern Hemisphere (SH), respectively. The identification procedure is illustrated in Fig. 2 for an NH TP. In the following, the three requirements for TPs are discussed in more detail:

1) As mentioned before, cold T_b values are an indicator for high cloud tops. The advantage of using anomalies instead of absolute values is to enhance the identification of transient systems rather than semipermanent features such as the SPCZ. The threshold of -20 K was chosen in comparison to subjectively identified TPs during a short test period. As expected, TP frequencies decrease markedly with higher thresholds. For -30 K, for instance, TP numbers are about halved.

2) The maximum extension of a TP event is defined as the length of the diagonal of the rectangle that connects the southernmost, northernmost, westernmost, and easternmost points of the TP (bold dotted line within the dotted rectangle in Fig. 2). A minimum length of 2000 km was chosen to detect cloud systems of at least synoptic scale.
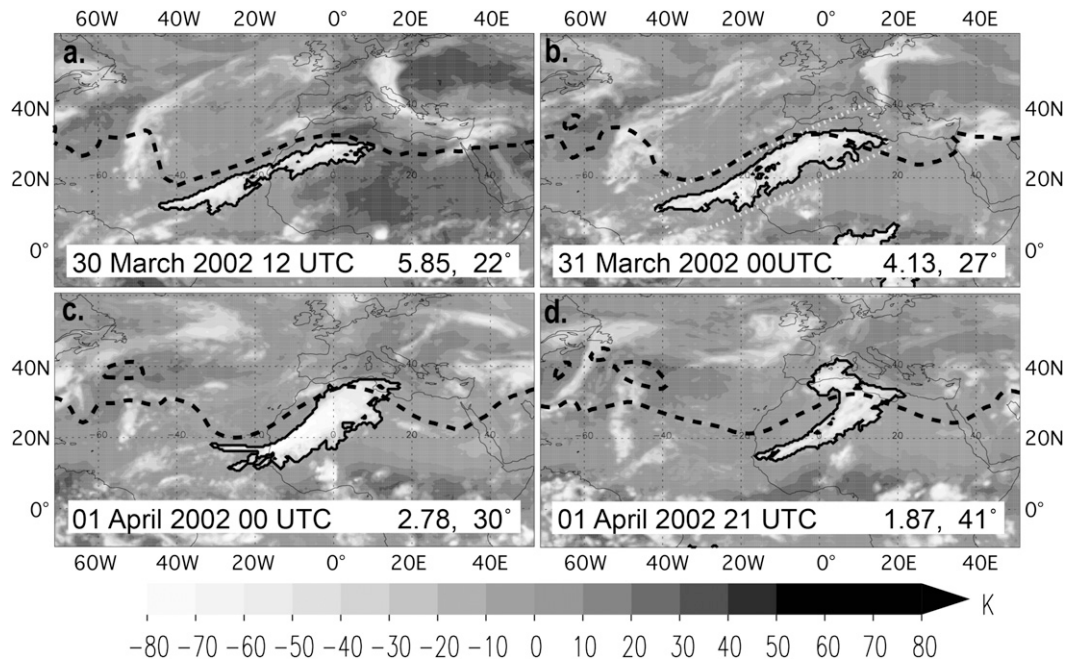
FIG. 3. Example TPs. Brightness temperature anomalies (K) for (a) 1200 UTC 30 Mar, (b) 0000 UTC 31 Mar, (c) 0000 UTC 1 Apr, and (d) 2100 UTC 1 Apr 2002. Detected TPs are marked with thick black contours. The dashed black contour is the 2-PVU contour of the vertically (100–400 hPa) averaged PV field. The numbers in the bottom-right corners are the LWR value and the estimated horizontal tilt (see section 2b). The dotted gray lines in (b) mark the smallest rectangle that contains the TP.

3) Cloud bands are required to cross 15°N or 15°S in order to filter out systems with a significant tropical–extratropical interaction.

All detected TPs are tracked based on spatial overlap. If a TP can be found for at least two consecutive analysis times (minimum lifetime of 3 h), the respective time period is defined as a TP episode. The TP lifetime is evaluated statistically in section 4. In addition, a length-to-width ratio (LWR) is introduced as a measure of the elongatedness of a cloud structure, which is computed for the smallest rectangle encompassing the TP (gray-filled rectangle in Fig. 2; real-world example in Fig. 3b). The LWR criterion is applied to TP episodes rather than to individual detected cloud bands to account for the fact that the shape of a TP changes during its lifetime with the elongated shape often only achieved at a mature stage. For the final TP climatology a maximum LWR of 3 is chosen to filter out convective systems with a rather circular or oval shape, as often found over continental monsoon regions in the outer tropics of the summer hemisphere. An even larger LWR threshold would have emphasized the elongatedness more, but the number of detected TPs decreases rapidly with increasing LWR value. Only 50% (10%) of the detected TPs would satisfy a LWR threshold of 4 (5). The smallest

surrounding rectangle employed for the LWR computation is also used to determine the tilting angle α between the TP and the equator (see Fig. 2). It should be pointed out that the described method is solely based on horizontal cloud structure and therefore not able per se to distinguish between mesoscale or larger convective systems or cloud bands that are produced mainly by advective or frontal processes (see discussion in Knippertz 2007).

c. Illustrative example

With the algorithm described above, a TP episode was detected over the North Atlantic from 1800 UTC 29 March to 900 UTC 2 April 2002. This event was briefly mentioned in the introduction with regard to the heavy rainfall over Morocco and Algeria it was associated with and is shown in Fig. 1. Figure 3 shows T_b anomalies, the identified TP structures (black lines), and the 2-PVU contour (dashed black line; vertically averaged between 100 and 400 hPa) for different analysis times within the lifetime of the TP of nearly 4 days. The TP is first detected over the central equatorial North Atlantic as a nearly east–west-oriented ($\alpha = 11°$) narrow cloud band (not shown). The TP then expands northeastward along the eastern edge of a subtropical upper trough,

(a) October to March
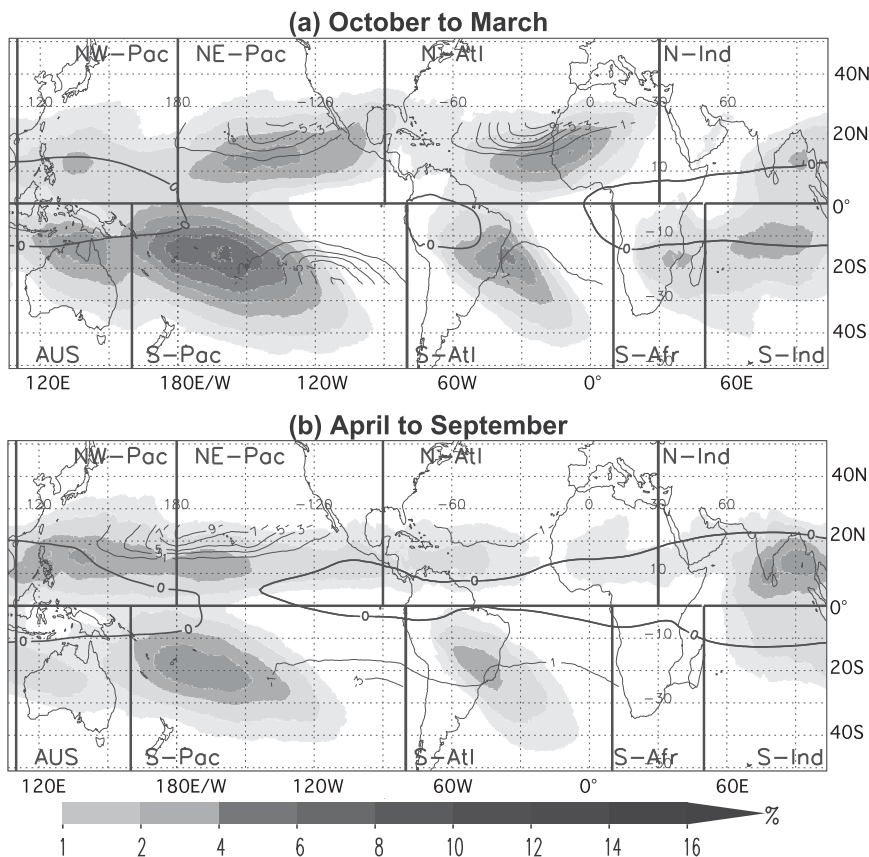

(b) April to September

FIG. 4. Mean TP frequency (%; shaded) for NH (a) Oct–Mar and (b) Apr–Sep between July 1983 and June 2006. The regions used for further investigations are indicated by black rectangles. The contours display the mean frequency of troughs at low latitudes (m s^{-1}) detected by Fröhlich and Knippertz (2008) in the ERA-40 data between 1980 and 2001. The bold gray contour presents the zero line of the mean zonal wind at 200 hPa from 1980 to 2001.

as evident in the 2-PVU contour in Fig. 3 (dashed black line). On 30 March (Fig. 3a), the detected TP extends over more than 6000 km from the central tropical North Atlantic into the subtropics over northwestern Africa with the typical anticyclonic curvature at its northeastern end found for other cases (McGuirk et al. 1987). At this time, the TP reaches its maximum LWR value of 5.85 and a tilting angle of 22°. In the next hours, the TP expands spatially and T_b anomalies become more negative, which points to higher cloud tops (Figs. 3b,c). At 2100 UTC 1 April (Fig. 3d), the TP extends into the Mediterranean Sea, where it begins to roll up cyclonically. The resulting lambda-shaped structure is related to the development of a low-level extratropical cyclone (Thepenier and Cruette 1981; Fink and Knippertz 2003). The temporal evolution and the relation to the upper subtropical trough are typical of TP developments over the North Atlantic/northwest African region in winter.

3. Climatological results

a. Geographical and seasonal distribution

The climatological distribution of the TP frequencies f_{TP} for the 23-yr investigation period from July 1983 until June 2006 is depicted in Fig. 4. Here, f_{TP} is the percentage of analysis times for which a respective grid point is part of a TP event. The distribution reveals nine well-defined areas of preferred TP formation, which are mostly located over oceans.

In boreal winter (Fig. 4a), a maximum of 12% is found over the western South Pacific in relation to the SPCZ. The f_{TP} maxima of nearly 9% are found over the North Atlantic and South Atlantic (related to the SACZ) and of nearly 7% over the eastern North Pacific and over northern Australia. The local f_{TP} maxima over the southern Indian Ocean, the western North Pacific, the Bay of Bengal, and southern Africa (related to the SICZ) have frequencies below 6%. The orientation of

the main f_{TP} maxima is in accordance with the majority of the individual systems (see section 4b). It is remarkable that the regions with highest TP frequencies in the NH (North Atlantic and eastern North Pacific) are located west of the main landmasses, while the opposite is true in the SH (western South Pacific and South Atlantic). Figure 4 also shows the mean frequency of upper-level troughs at low latitudes as detected by Fröhlich and Knippertz (2008) for the period 1980–2001 (thin contours). This climatology shows frequency maxima in regions where westerly winds are predominant over the equator (westerly ducts, thick contours, averaged between 1980 and 2001). Over the North Pacific and North Atlantic TPs preferentially develop to the southeast of the main trough activity centers in contrast to the South Pacific and South Atlantic. This likely reflects the differences of the genesis of diagonal cloud bands that is largely related to lifting ahead of low-latitude troughs in the two former regions and to diagonal subtropical convergence zones (i.e., SPCZ and SACZ) in the latter two. In the SPCZ and SACZ region, low-latitude troughs are observed downstream of the TP.

In boreal summer (Fig. 4b), the geographical distribution in the SH is quite similar, although the magnitudes are strongly reduced, especially over southern Africa and the southern Indian Ocean. In the NH, seasonal changes are more pronounced: while f_{TP} increases over the western North Pacific, India, and the Bay of Bengal, TP occurrence is reduced and shifted westward over the North Atlantic and eastern North Pacific. The west–east orientation of the f_{TP} maxima in these regions suggests that the detected TPs might reflect segments of the northward-shifted ITCZ. This may also be the reason for the slight increase in TP occurrence over eastern North Africa and the Arabian Peninsula.

An integral way to describe the geographical distribution of TPs is to compare regional TP frequencies. For this purpose, nine regions of high TP activity were subjectively defined on the basis of the winter climatology (black boxes in Fig. 4). The four regions in the NH and the five regions in the SH are as follows: the northern Indian Ocean (N-Ind: 30°–110°E), western North Pacific (NW-Pac: 110°E–180°), eastern North Pacific (NE-Pac: 180°–90°W), North Atlantic–northwestern Africa (N-Atl: 90°W–30°E), southern Indian Ocean (S-Ind: 50°–110°E), Australia (Austr: 110°–160°E), South Pacific (S-Pac: 160°E–80°W), South Atlantic (S-Atl: 80°W–10°E), and southern Africa (S-Afr: 10°–50°E). Note the different size of the boxes. For calculating regional TP frequencies each TP is assigned to one of these regions according to its southernmost point. TP events that extend across the equator (about 17% of all TP events) are assigned to the hemisphere where most of the cloud
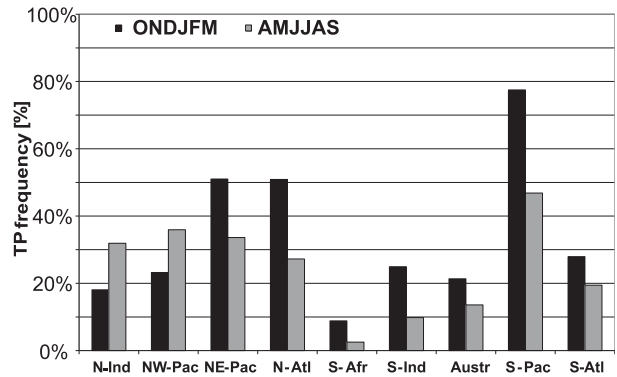

FIG. 5. Boreal-winter (black) and boreal-summer (gray) mean TP frequencies (%) per region for the period July 1983–June 2006. Regions are defined in Fig. 4.

structure is detected. Consistent with the gridpoint-based analysis, regional TP frequencies are generally higher in boreal winter except for the N-Ind and NW-Pac regions (Fig. 5). Maximum TP frequencies during this time of year are found in the S-Pac (77.5%), followed by NE-Pac (51.0%) and N-Atl (50.9%). Globally, nearly three (two) TP events are detected on average at each analysis time in boreal winter (summer).

Monthly mean TP frequencies for these regions (Fig. 6) reveal three major types of seasonal behavior: (i) maxima in the transition seasons (N-Atl, NE-Pac, and S-Atl), typically with high values throughout the boreal-winter half-year; (ii) maxima in boreal summer in the NH monsoon regions (NW-Pac and N-Ind); and (iii) maxima between October and March in the SH (S-Pac, S-Afr, Austr, and S-Ind).

With respect to the geographical and seasonal distribution of TP frequencies, the presented climatology largely agrees with results documented in previous studies (Thepenier and Cruette 1981; McGuirk et al. 1987; Kuhnel 1989; Iskenderian 1995) but adds a lot more statistical robustness to the results, as it covers the whole globe for a much more extended time period in an objective way. To better illustrate this, Fig. 7 summarizes the results by Kuhnel (1989) (global) and Iskenderian (1995) (only NH). The high TP activity over the central and eastern North Pacific and North Atlantic during NH winter found by Iskenderian (1995) is in close agreement with Fig. 4. The 14 TP regions defined by Kuhnel (1989) (seven in each hemisphere; see Fig. 7) have clear overlap with the nine TP regions used in this work. Kuhnel's climatology is also dominated by high TP numbers over the SPCZ and SACZ. McGuirk et al. (1987) find maxima in cloud band activity over the central and eastern North Pacific in November and April and a relative minimum from February to March in agreement with the NE-Pac results in Fig. 6a.
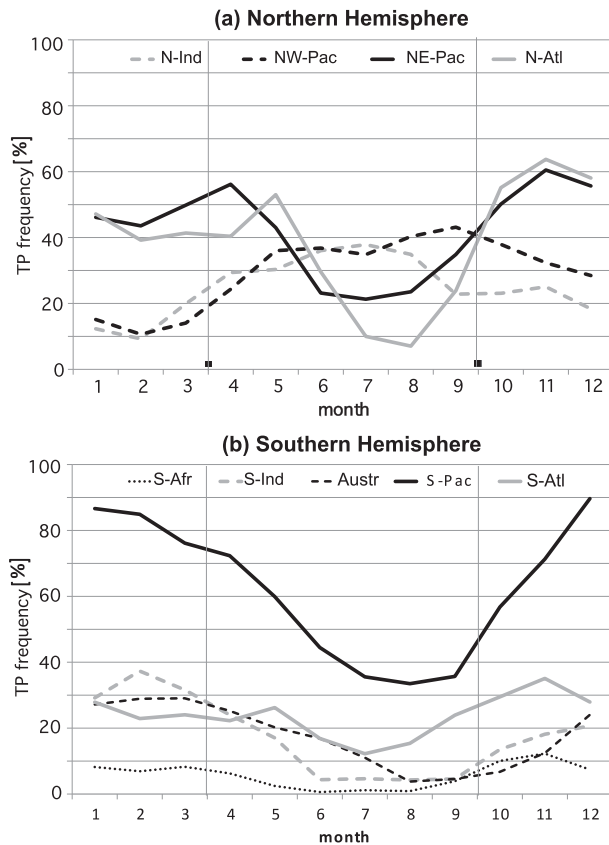
FIG. 6. Monthly mean TP frequencies (%) for the study regions in the (a) NH and (b) SH averaged between July 1983 and June 2006. Regions are defined as in Fig. 4.

b. Sensitivity to the identification method

In this subsection, the sensitivity of the TP identification algorithm to (i) the implementation of the LWR criterion and (ii) the employed data basis is briefly assessed. To estimate the influence of the former, TP frequencies without LWR restriction are depicted in Fig. 8a for boreal winter. The geographical distribution resembles that of the original TP climatology in Fig. 4a, but frequencies are generally higher with maxima over the South Pacific and South America/South Atlantic region of more than 13%. Regarding regional TP event numbers, the highest fraction (about 70%) of TPs that satisfy the LWR criterion are found in the westerly duct regions, such as the N-Atl, NE-Pac, and S-Pac regions (not shown). The greatest differences between the two climatologies are observed in regions, where more circular cloud structures in relation to tropical convective processes are expected to be predominant (S-Afr, S-Ind, N-Ind, and NW-Pac). For example, only about 30% of the detected S-Afr cloud bands in austral summer are part of a TP episode with a maximum LWR value of 3 or

more. Tests with higher LWR thresholds emphasize these differences in the TP distribution even more (not shown). Changes in the other TP identification thresholds (i.e., T_b anomaly, maximum extension, and crossing latitude) generally produce TP climatologies with similar geographical and seasonal distributions but with different magnitudes in the total TP numbers (not shown).

To evaluate the influence of the data basis, the identification algorithm (here without LWR criterion) was also applied to the PATMOS-x T_b data (Fig. 8b). The resulting climatology is structurally similar but characterized by much lower TP frequencies with a global maximum of less than 5% over the western South Pacific. The strongly reduced numbers are most likely explained by the finer spatial and coarser temporal resolutions. Discontinuities in the cloud bands are better resolved and violate the criterion of spatial contiguity, while those due to the daily resolution short-lived TPs are missed. Overall, the analyses in this section have demonstrated that the geographical distribution of the most active TP regions is a robust feature despite of the sensitivity of the TP identification to the choice of the individual thresholds, the data basis, and other details of the detection algorithm.

4. TP characteristics

a. Lifetime

In the following section, TP episodes are analyzed with respect to geographical and seasonal variations in their frequency and lifetime. A TP episode is assigned to one of the regions used in section 3 (see Fig. 4) according to the location of its southernmost point at first appearance. The mean number of TP episodes per season and their mean lifetime are displayed in Fig. 9. Recall that the minimum lifetime of a TP is 3 h. As expected, the geographical distribution resembles that of TP events (Fig. 5). In boreal winter, TP episodes are most frequent in the S-Pac region with 62 episodes on average per winter (black bars in Fig. 9) followed by the N-Atl region with 57 episodes. During boreal summer, the geographical distribution of TP episodes is rather similar, although absolute numbers are much reduced, except for the N-Ind and NW-Pac region.

The definition of TP episodes is similar to prior studies, which often consider cloud bands from the beginning to the end as one cloud system and therefore allows a comparison of absolute numbers: McGuirk et al. (1987) detected an average of 48 cloud plumes per winter (November–April) over the eastern North Pacific (180°–90°W), which is in remarkable agreement with the
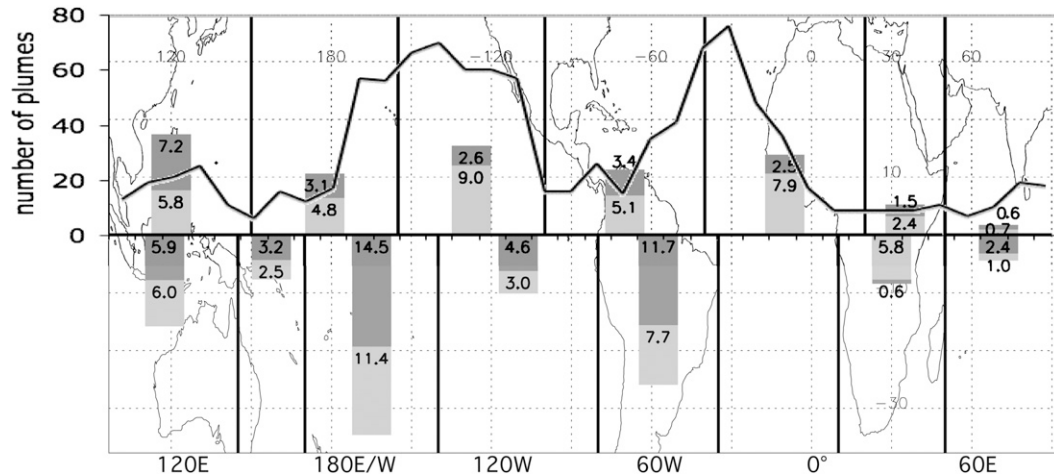
FIG. 7. The TP distribution from the climatologies of Kuhnel (1989) (bars) and Iskenderian (1995) (line; NH only). The bars show the mean monthly TP frequency (number of days with TP occurrence) for 14 regions between 1979 and 1983. Lighter (darker) gray boxes present the winter (summer) TP frequencies in the respective hemisphere. The two seasons are based on the periods October–March and April–September. The line displays the number of plumes in 10° longitude bands for the years 1974–1984 between October and May according to the y axis on the left-hand side.

present study (NE-Pac: 46 between October and March). Iskenderian (1995) observed on average 106 TPs per winter season (October–May) in the NH: 40 of which are in the eastern North Pacific. While the latter is in reasonable agreement with the present climatology, the former is only about 70% of what is found here. The differences are likely due to the twice-daily temporal resolution used in Iskenderian (1995) that misses out on shorter-lived TPs outside of the North Pacific basin.

The black and gray dots in Fig. 9 indicate mean TP lifetime. The global mean is 1.6 days. On average TPs are more persistent during boreal winter than summer and in the SH than in the NH. The maximum TP duration of nearly 2.5 days is found in the Austr region during austral summer, where more than 4% of all episodes persist 10 days or longer, with 6 even lasting longer than 20 days. SW-Pac has the second longest lifetime during boreal winter of about 2.2 days and with more than 3% of all TP episodes lasting longer than 10 days. In the NH, the regional mean lifetimes vary between 1.5 and 2 days during boreal winter. Only 0.8% (26) of all TPs in the NH live 10 days or more. During boreal summer, the mean lifetime is reduced in most regions, except for the S-Afr and NW-Pac regions. In the latter, TPs persist for 2.2 days on average and more than 3% last longer than 10 days.

The mean duration of cloud bands in the North Pacific sector estimated by McGuirk et al. (1987) and Iskenderian (1995) is around 2.6 days. This is somewhat longer than the NE-Pac value found in this study (1.8 days). This is presumably due to the differences in detecting the first appearance of a TP. McGuirk et al.

(1987) define the time of beginning as "the first evidence of poleward progression of the cloud mass which later develops into a moisture burst." This means that a cloud band is already detected before it satisfies the actual TP definition, in contrast to the procedure applied in this work. Furthermore, while in the study of McGuirk et al. (1987) most of the cloud bands last 2–4 days, in the present climatology nearly 50% of all detected TP last 1 day or shorter, which is likely due to the higher temporal resolution used here. It is also worth noting that the fraction of long-lived TPs increases with higher maximum LWR values of the TP episode (not shown).

b. Horizontal tilt

The horizontal tilt of a TP is defined by the angle α between the smallest surrounding rectangle and the equator (Fig. 2). The term α is zero for west–east-oriented cloud bands and positive (negative) for southwest–northeast (northwest–southeast)-oriented TPs. The tilting angle provides some insight into the likely origin of TP genesis. More meridionally oriented TPs (positive α in the NH; negative α in the SH) point to a genesis in relation to transient upper trough occurrence, whereas more zonally oriented TPs might rather be related to poleward displaced ITCZ segments in summer monsoon regions or to very strong wave breaking in the subtropics. The orientation of the TP will also affect meridional eddy fluxes of heat, moisture, and momentum (Kiladis and Weickmann 1992).

A normalized distribution of α shows that as expected most of the TPs in the NH are positively tilted (Fig. 10a)
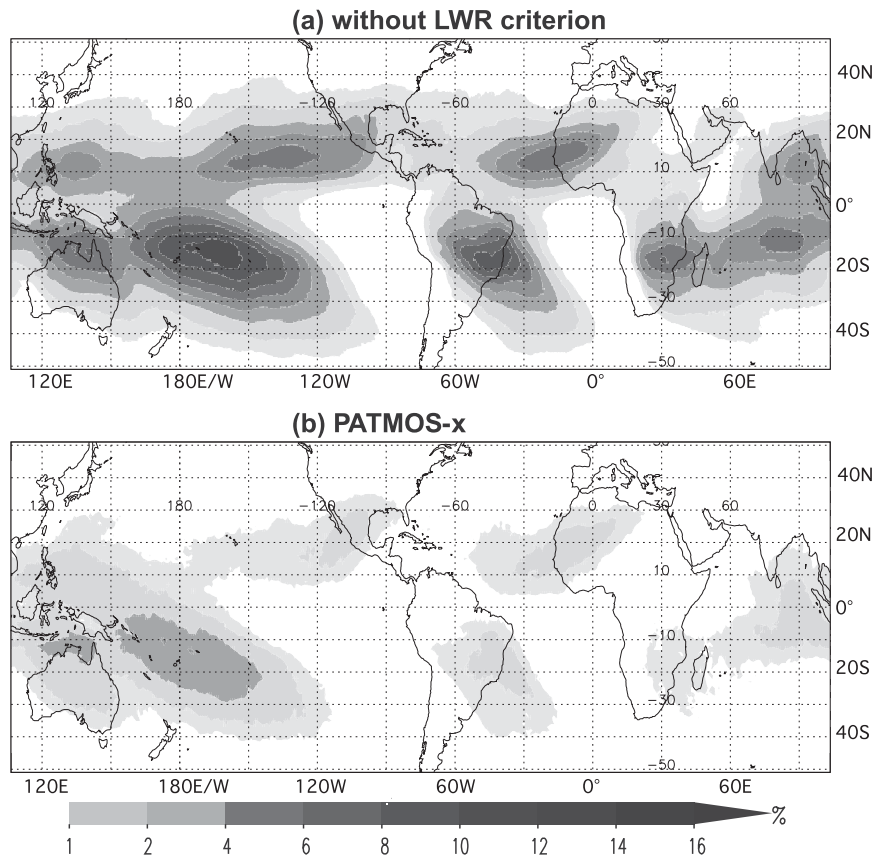
(a) without LWR criterion

(b) PATMOS-x

FIG. 8. As in Fig. 4a, but for cloud structures identified without applying the LWR criterion based on (a) CLAUS and (b) the PATMOS-x T_b dataset.

and in the SH are negatively tilted (Fig. 10b). Maximum TP frequencies are observed between 20° and 40° in the NH during winter and summer with a slight tendency to larger tilts in winter (Fig. 10a). A second maximum appears during summer for tilting angles between 0° and 10°, which points to an increase of nearly west–east-oriented northward-shifted segments of the ITCZ, in particular in the NE-Pac region. In the SH, most TP events are characterized by tilting angles between −50° and −30° in austral summer and between −40° and −20° in winter (Fig. 10b), which implies that austral-summer TPs in the SH have a slightly greater angle toward the equator than NH events and austral-winter SH events. Overall, the distribution of α, especially on a regional scale (not shown), corresponds well with the orientation of the main f_{TP} maxima in the gridpoint-based TP climatology in Fig. 4.

5. Interannual variability

In this section, interannual variations in the TP frequencies are examined, primarily in association with

ENSO. For these investigations, two TP composites were constructed on the basis of six El Niño and five La Niña winters (Figs. 11a,b). Furthermore correlations between the gridpoint-based TP frequencies and the Niño-3.4 index were calculated and are depicted in Fig. 11c together with the differences between the two ENSO phases. ENSO-induced fluctuations are most pronounced over the Pacific Ocean with correlations of more than |0.8| very close to the main activity region of ENSO (Fig. 11c). During El Niño events, TP frequencies increase in a large area over the tropical central and eastern North Pacific (Fig. 11a), in agreement with a shift of the main convective regions. Interestingly, TP activity expands much farther into the Gulf of Mexico and western North Atlantic during El Niño events. Over the western South Pacific, a dipole of positive and negative correlations with a sharp northwest–southeast-oriented boundary is evident (Fig. 11c), which indicates an eastward shift of TP occurrence during El Niño (leading to a corresponding shift of the SPCZ as discussed in Vincent 1994). The southern Indian Ocean and the region from the subtropical eastern North Pacific to
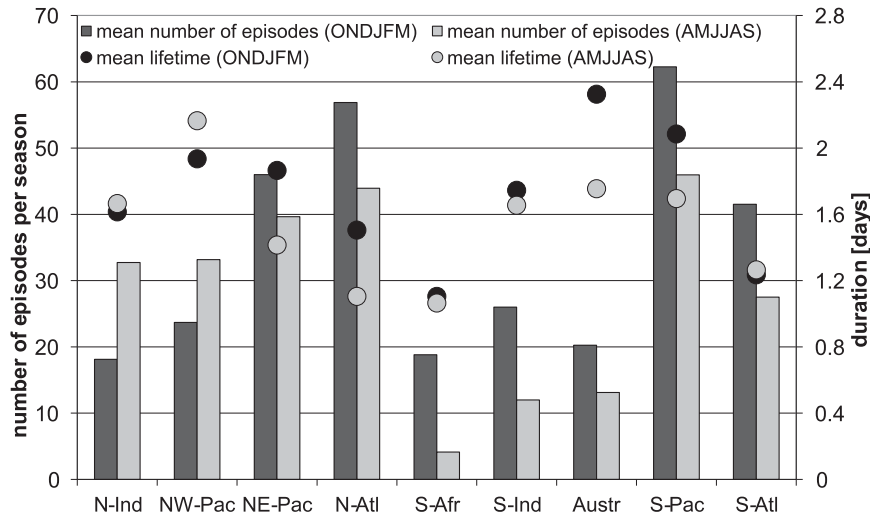
FIG. 9. Mean number of TP episodes per season (bars; left *y* axis) and mean TP lifetime in days (circles; right *y* axis) during the period July 1983–June 2006 for the regions defined in Fig. 4. The NH winter is black and summer is gray.

the Gulf of Mexico show significant positive correlations (Fig. 11c): that is, enhanced TP activity during the warm phase of ENSO (Fig. 11a).

Correlations between TP frequency and other climate state indices such as the NAO and PNA are generally low (not shown), except for NW-Pac and Austr, which show significant negative correlation with the PNA index. It is likely that these strong links are moderated by ENSO (e.g., Straus and Shukla 2002). ENSO-related changes in the TP frequencies were already suggested by McGuirk et al. (1987), who found reduced numbers of TPs over the eastern North Pacific in the strong El Niño winter of 1983/82.

Evan et al. (2007) found significant negative long-term trends in cloudiness in the ISCCP dataset, which the authors explain by inhomogeneities in the satellite viewing geometries (i.e., limb darkening) rather than a reflection of real atmospheric changes. A regional trend analysis for TP frequencies on the basis of the CLAUS dataset also show a significant downward trend with the strongest signals in the N-Ind, S-Ind, and S-Atl regions, most likely for the same reasons as in Evan et al. (2007). A trend analysis with the more homogeneous PATMOS-x data in contrast does not yield any significant long-term trends (not shown).

6. Mechanisms

To better understand the physical processes leading to TP genesis, upper-level circulation anomalies are investigated in this section based on a system-relative composite analysis to maximize signal strength. Composite

maps of vertically averaged (between 100 and 400 hPa) PV (VAPV) anomalies centered on the latitude of the central point of a TP (i.e., the mean latitude of all grid points within the TP) at the first time of detection were constructed for all TP episodes identified between July 1983 and December 2001, the overlap period of the CLAUS and ERA-40 data. The statistical significance of the system-relative composites is estimated using a Monte Carlo calculation, which is described in detail in Moore et al. (2008) and includes a comparison of the composite fields with 300 composites based on randomly selected analysis fields. Only values above the 95% level are shown. Figure 12 shows the results for eight high-TP activity regions for boreal winter together with T_b anomalies of less than -5 K (contours) averaged over the respective composite to represent the position and shape of the mean TP.

In most of the NH regions, a positive PV anomaly is evident to the west of the TP, which is part of a northwest–southeast-oriented wave train. This points to TP development along the eastern flank of an upper-level trough with extratropical origin. This signal is most pronounced in NE-Pac (Fig. 12c), broadly in agreement with Iskenderian (1995) and Kiladis and Weickmann (1992, their Fig. 2), who argue that cloud systems in the eastern Pacific are forced by transient Rossby waves that originate in the East Asian subtropical jet region and propagate southeastward from the midlatitudes through the westerly duct in the eastern Pacific. A similar wave train (with lower amplitudes) is apparent in the N-Atl, S-Atl, S-Pac, S-Ind, and S-Afr regions (Figs. 12d–h). In the SH regions, the PV trough directly related to TP genesis is

(a) Northern Hemisphere

■ NH (ONDJFM #42687)   ■ NH (AMJJAS #37142)

(b) Southern Hemisphere

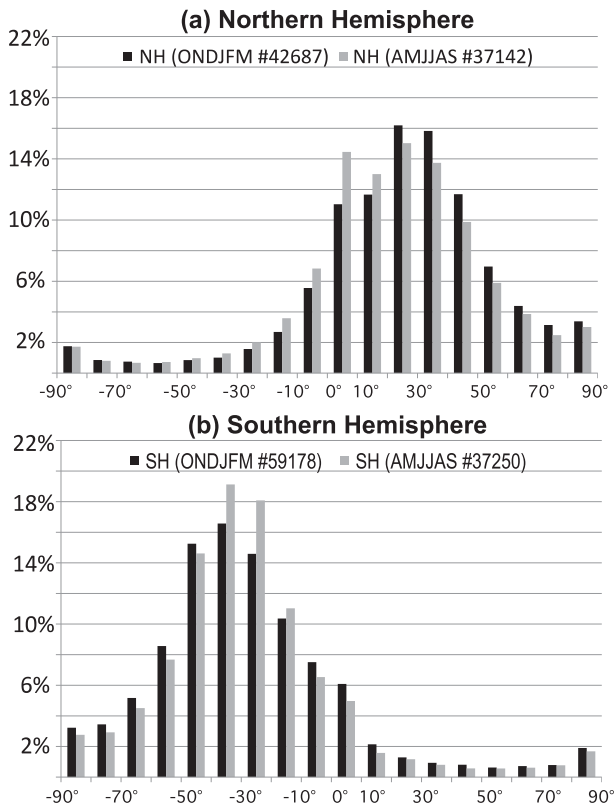■ SH (ONDJFM #59178)   ■ SH (AMJJAS #37250)

FIG. 10. Normalized distribution of TP horizontal tilt for TPs detected in (a) the NH and (b) the SH. The black (gray) bars show boreal-winter (summer) frequencies of the period July 1983–June 2006. The total numbers for each season and region are given in parentheses.

located farther away from the equator than the respective NH troughs, which is likely related to a mean position of the ITCZ south of the equator during boreal winter.

The N-Ind and NW-Pac composites (Figs. 12a,b) exhibit a significant downstream development as indicated by a wave structure at about 40°N to the east of the TP. These results are consistent with circulation anomalies found by Kiladis and Weickmann (1997, their Fig. 4b) in relation to enhanced convection in the western tropical North Pacific. They suggest that divergent outflow from the region of enhanced convection leads to the generation of a subtropical anticyclone, which acts as a Rossby wave source for an eastward-propagating midlatitude wave train. Lagged relationships (not shown) suggest that these circulation anomalies are strongest after the convection anomaly peaked, which implies that the circulation is forced by the convection (Kiladis and Weickmann 1997).

Figure 12 reveals that in the majority of the regions cold clouds associated with TPs are the result of

equatorward-propagating Rossby wave trains. This is no surprise for the regions of mean upper-level westerlies (NE-Pac, N-Atl, S-Pac, and S-Atl), where such a connection has been documented in many studies. However, for regions with mean upper-level easterlies such a connection was not expected but is seen in Figs. 12a,b for the N-Ind and NW-Pac regions. Kiladis and Weickmann (1997) suggested that the convection in these regions is mainly associated with patterns of meridional outflow into subtropical anticyclones. Although this is also evident in Figs. 12a,b, the results shown here suggest both a wave train from the extratropics approaching the TP feature from the west and a wave train emanating from the TP feature toward the extratropics to the east. This is especially pronounced for the N-Ind region (Fig. 12a). It is conceivable that these differences arise from the implementation of the LWR criterion (see section 2), which requires an elongated shape of the cold cloud anomalies. This idea is confirmed by looking at composites of upper circulation anomalies based on TP episodes with LWR values less than 3 (not shown), which generally show enhanced downstream development. Consequently, elongated cloud bands appear to be the result of cloud anomalies induced by transient upper-level troughs from the extratropics despite the mean upper easterlies.

7. Impacts on radiation and moisture distribution

As discussed in the introduction, TPs have been described to be connected with poleward transports of tropical moisture and precipitation in the extratropics and can be expected to affect the earth's radiation budget locally and globally. These effects have never been quantified and will be discussed in this short section.

a. Impacts on radiation

Averaging the TP climatology presented in section 3 yields a mean annual TP coverage of about 3.5% in the tropics (between 30°S and 30°N). It is not trivial to estimate the albedo of TPs, as they can consist of a wide range of cloud types reaching from deep tropical convection with an albedo of up to 0.9 to thin cirrus with values as low as 0.2 (McGuirk et al. 1987, 1988) (for a cross section along a modeled TP cloud band, see Knippertz 2005). To get a rough estimate of the global and tropical albedo effect of TPs, we simply assume that a removal of all TPs would on average reduce the local albedo by about 0.5, as the majority of TPs occurs over dark ocean surfaces (see Fig. 4). Combined with the 3.5% average coverage mentioned above, this yields a reduction of the tropical albedo by 0.018. Given that the 30°S–30°N band covers about 61% of a disk

(a) El Niño

(b) La Niña

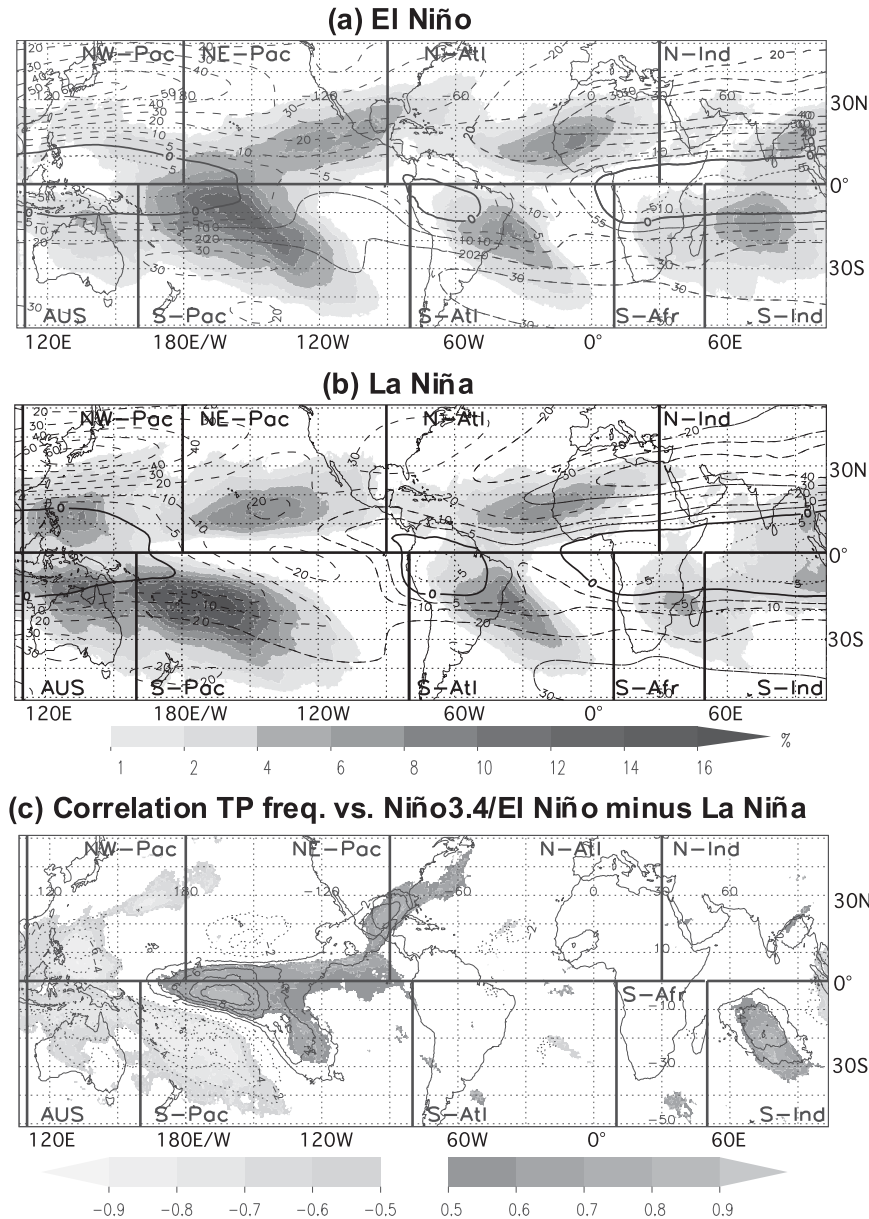## (c) Correlation TP freq. vs. Niño3.4/El Niño minus La Niña

FIG. 11. Mean TP frequency (%; shaded) averaged between October and March for (a) six El Niño winters (1986/87, 1987/88, 1991/92, 1994/95, 1997/98, and 2002/03) and (b) five La Niña winters (1984/85, 1988/89, 1995/96, 1998/99, and 1999/2000). The contours in (a) and (b) display the mean zonal wind at 200 hPa (m s^{-1}; dashed contours for westerlies and dotted contours for easterlies with the zero contour in bold) based on ERA-40 data between 1980 and 2001. (c) Correlation coefficients between TP frequencies and the Niño-3.4 index in winter (October—March, shading). Only significant (99% level) correlations are shaded. Contours are differences of (a) minus (b).

perpendicular to the incoming solar radiation, the corresponding global value would be a small but not insignificant reduction of 0.011 or ~0.29 instead of the observed 0.3.

Estimating the impact of TPs on the earth's radiation budget is more difficult, as longwave effects have to be taken into account as well. The optical depth of the different cloud types TPs typically consist of stretches over two orders of magnitude or more. For the often dominating altostratus and cirrostratus clouds, optical depths range from about 1 to 10, giving a net radiative cloud forcing between +38 and −30 W m^{-2} for 12-km

(a) N-Ind

(b) NW-Pac

(c) NE-Pac

(d) N-Atl

(e) S-Afr
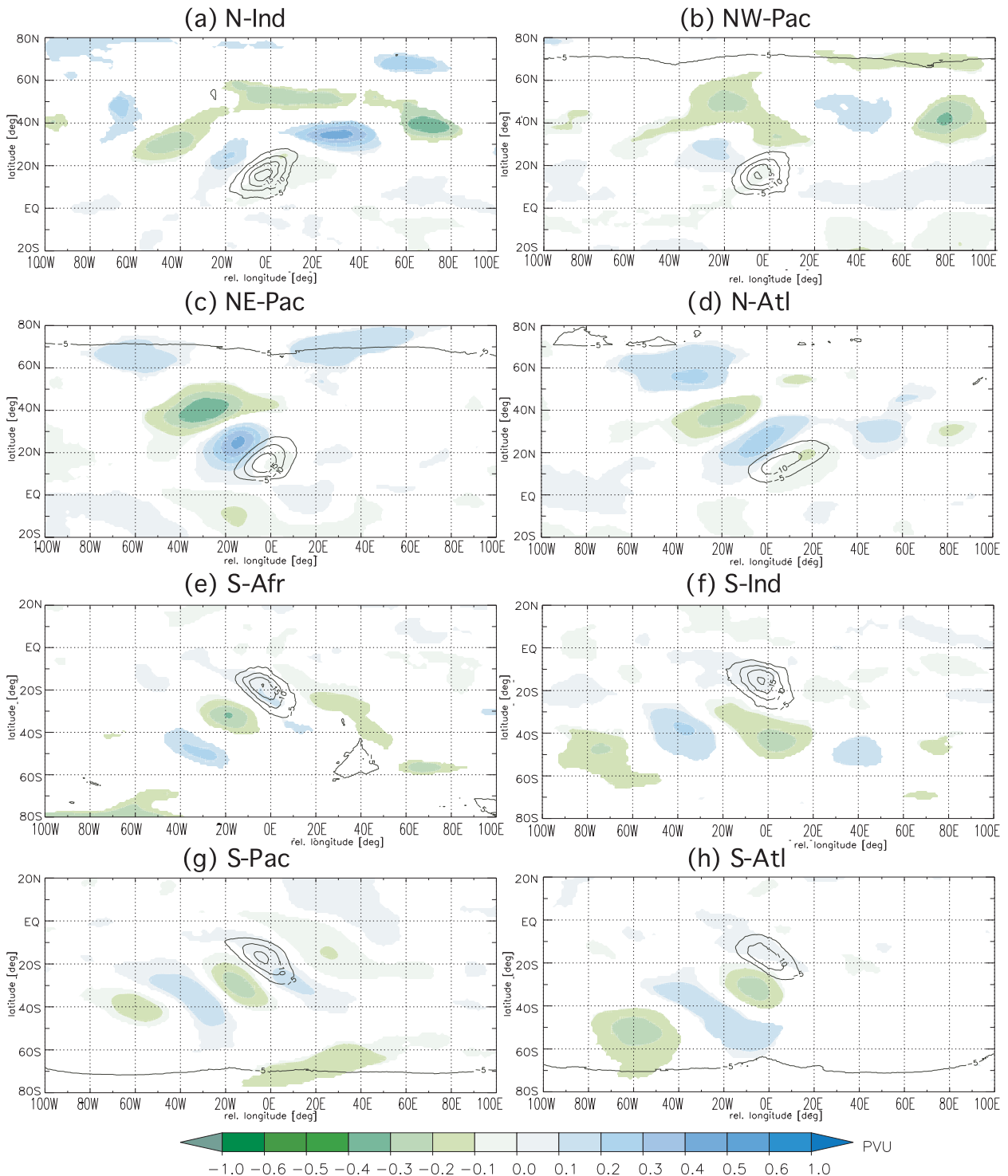
(f) S-Ind

(g) S-Pac

(h) S-Atl

FIG. 12. Composites of statistically significant (95% level) VAPV anomalies (PVU; shaded) and negative T_b anomalies (K; contours) < -5 K (indicator for the mean TP) for TP episodes in the (a) N-Ind, (b) NW-Pac, (c) NE-Pac, (d) N-Atl, (e) S-Afr, (f) S-Ind, (g) S-Pac, and (h) S-Atl during boreal winter (October–March) from 1983 to 2001.

cloud top under tropical conditions (Corti and Peter 2009). This implies that dependent on optical depth TPs or parts of TPs can lead to a warming or cooling of the earth–atmosphere system with the net effect hard to assess without substantial further data analysis or modeling.

A study by Harrison et al. (1990), who analyze the impact of clouds on the earth's radiation budget based on data from the National Aeronautics and Space Administration (NASA) Earth Radiation Budget Experiment, provides a nice illustrative example. The authors present maps of the albedo and longwave and shortwave cloud radiative forcing averaged for January 1986. In all of these plots, a southwest–northeast-oriented, TP-like structure appears over the tropical North Atlantic, suggesting high TP activity in that region and month as confirmed by the CLAUS data. The net cloud forcing for January 1986 displays only a weak and inhomogeneous signal over this region (their Fig. 5b). While the southwestern part of the TP structure is characterized by a negative net cloud forcing (probably optically deep convective clouds near the ITCZ), the northeastern part has positive values (thin cirrus). To assess the full radiative impact of TPs, the longwave effects of anomalies in moisture in cloud-free regions would have to be taken into account as well as (see discussion in section 7b) as in the case study presented by Knippertz and Fink (2008).

b. Impacts on moisture distribution

The identification of TPs used here is based on elongated regions of cold cloud tops. As shown in the previous section and many other studies (e.g., McGuirk et al. 1988; Iskenderian 1995), TPs are often associated with marked circulation anomalies at upper-tropospheric levels, while signals in the lower troposphere or midtroposphere, where the bulk of the moisture transport occurs, might be weaker or decoupled from the upper cloud band (Knippertz and Martin 2005, 2007; Ralph et al. 2011). Therefore, the occurrence of a TP is not necessarily representative of regions of strong water vapor transport from a column-integrated standpoint. A nice illustration of this is Fig. 3 of McGuirk et al. (1988) that shows a rare sounding-based observational analysis of such separation. Another indication is the opposite seasonality in the occurrence of TPs and atmospheric rivers (ARs) in the eastern North Pacific. While, according to Fig. 6a of the present paper, TP occurrence is most frequent during the boreal cool season with monthly maxima in April and November, the frequency of atmospheric rivers affecting the North American coast clearly peaks in summer (Neiman et al. 2008, their Fig. 2). This is consistent with the fact that many of these summertime ARs are not connected to exports of

tropical moisture (Roberge et al. 2009; Knippertz et al. 2013).

To quantify this aspect further, Fig. 13 shows anomaly composites of integrated water vapor (IWV) associated with TP occurrence in analogy to Fig. 12. In most regions, substantial IWV anomalies on the order of 4 g m^{-2} are found underneath and slightly to the west of the TPs. This displacement is consistent with the TP signatures including high clouds that have been blown poleward and eastward from a region of deeper clouds tied to lower-tropospheric water vapor (sometimes associated with an AR). Apart from the S-Pac region (Fig. 13g), which is influenced by the quasi-permanent SPCZ, significant anomalies do not stretch much beyond 30°N/S, which in a climatological sense supports the differences in the nature of TPs and atmospheric rivers discussed above. A striking exception is the NE-Atl region, where the IWV anomalies are weak and shifted far westward (Fig. 13d). A likely reason for this is the extension of many TPs in this region across the dry continental parts of northern Africa (see Fig. 4). As expected, wave trains from the extratropics are generally less evident than at upper levels (Fig. 12) and are most clear in NE-Pac, S-Pac, and S-Ind. In contrast, the N-Ind region shows a clear wave pattern in the NH tropics (Fig. 13a), which is not evident from VAPV (Fig. 12a). The zonally elongated dry anomalies in equatorial zones for the NW-Pac, NE-Pac, S-Pac, and S-Atl regions suggest that large-scale variability along the ITCZ may favor TP occurrence in certain regions. A detailed analysis of this aspect, however, is beyond the scope of this paper.

8. Summary and conclusions

In this study, an objective identification algorithm for TPs was developed on the basis of gridded T_b data. Following the classical definition of McGuirk et al. (1987), TP events are defined as extended bands (length > 2000 km) with T_b anomalies below −20 K that cross 15°N or 15°S. The detected systems were tracked in time to define TP episodes. Additionally, a criterion for the elongatedness of a cloud structure was implemented, which is based on the LWR of the smallest rectangle that contains the TP. Finally, only those TP events are retained that are part of a TP episode with a minimum time duration of 3 h and a maximum LWR value of 3 or more.

Applying the algorithm to the CLAUS T_b dataset, the first ever long-term objective climatology of TPs was constructed. Seasonal and geographical variations are largely in agreement with previous manual TP climatologies (McGuirk et al. 1987; Kuhnel 1989; Iskenderian 1995), but the results shown here are global, have
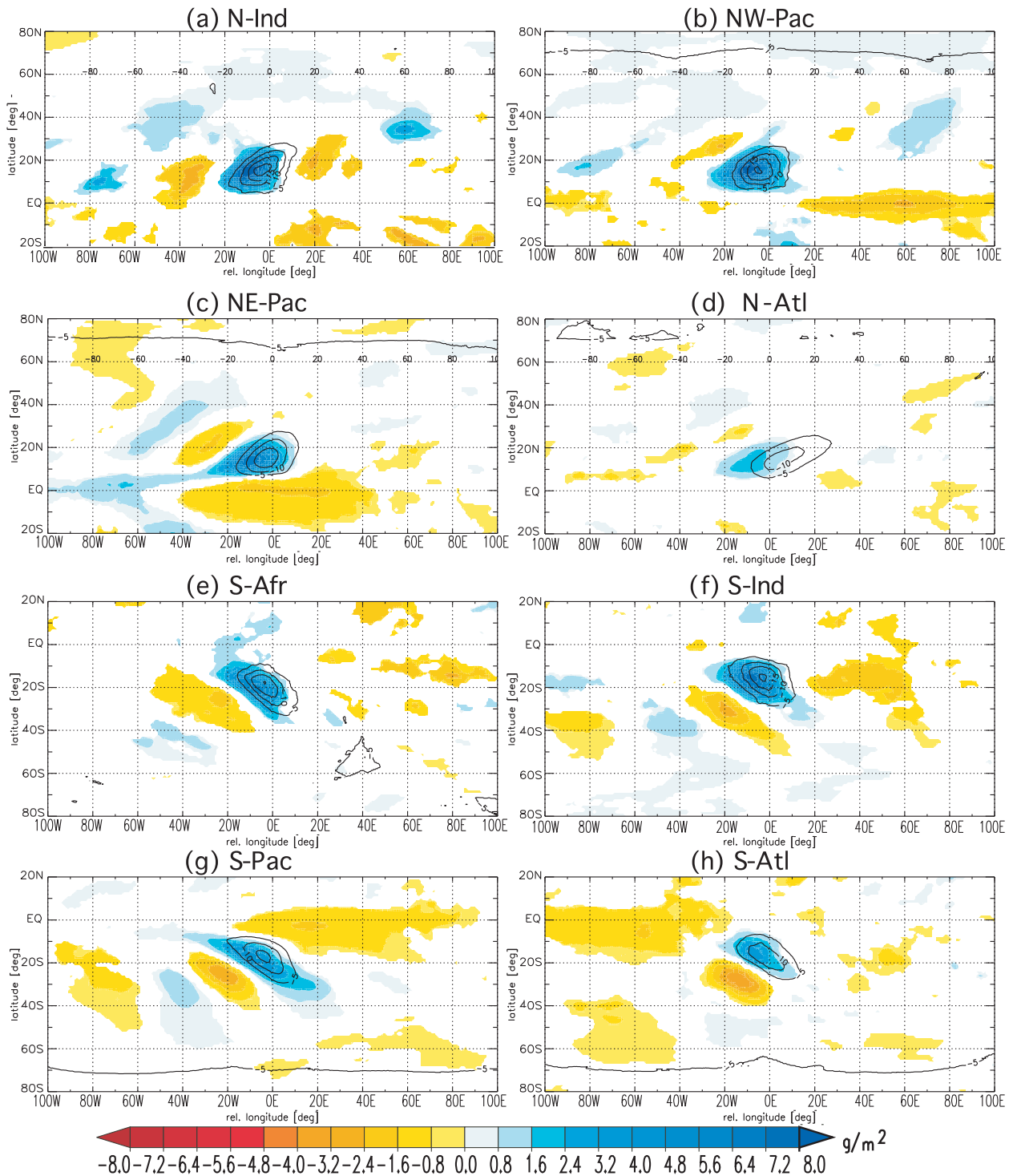
FIG. 13. As in Fig. 12, but for integrated water vapor anomalies (g m^{-2}; shaded).

a higher temporal resolution, cover a much longer period, and are therefore statistically much more robust. The main features of this novel TP climatology are as follows:

1) There are nine preferred TP regions with the global maximum located over the central South Pacific close to the SPCZ during boreal winter. Other maxima during this season are found over the eastern

parts of the North Pacific and North Atlantic Oceans and over the South Atlantic near the SACZ. In boreal summer, the geographical distribution of TP occurrence is similar, although TP frequencies are generally reduced except for the monsoon-influenced Bay of Bengal and the western North Pacific.

2) TP episodes last nearly 1.6 days on average. The most persistent TPs are found over Australia during austral summer with a mean duration of nearly 2.5 days. In this region, more than 4% of all TPs persist for 10 days or longer.

3) Most of the detected TPs are diagonal, which means that they are oriented southwest–northeast in the NH and northwest–southeast in the SH.

4) Interannual variations in boreal-winter TP frequency are related to ENSO, primarily over the Indo-Pacific region with a maximum correlation with the Niño-3.4 index found over the western North Pacific. Relations to the NAO and PNA are generally weak. No clear temporal trend can be detected with the datasets used here.

5) The elongated TP cloud bands are associated with transient upper-level troughs from the extratropics even in regions with mean upper easterly winds in the tropics. This is surprising given that the linear theory of stationary Rossby waves (Hoskins and Ambrizzi 1993) requires westerlies for wave propagation. It is not clear whether there are occasional westerly episodes on synoptic or intraseasonal time scales or whether the linear Rossby wave theory is too simplistic to describe the wave propagation.

6) TPs contribute on the order of 0.01 to brightening the earth's albedo, but estimating their net cloud radiative forcing is not possible based on this climatology alone.

7) TPs are generally associated with significant IWV anomalies in the subtropics only, which suggests that they are not necessarily associated with moisture transports to midlatitudes.

The TP identification presented here is sensitive to the choice of the employed thresholds and the time and space resolution of the input dataset. This mainly affects TP numbers and less so geographical structures. Most notably, the implementation of the LWR criterion reduces TP frequencies more strongly in regions where circular cloud structures are predominant such as over southern Africa and the Indian and northwestern Pacific Oceans. Such circular cloud structures are often related to poleward displaced ITCZ segments in monsoon regions. However, synoptic transient activity within the diagonal portion of the SPCZ and the SACZ is not filtered out by the applied criteria as evidenced by main

TP maxima in these two regions. The contribution of other tropical weather systems such as (recurving) tropical cyclones in the northwestern Pacific is much harder to determine and left for future study.

It is concluded that, despite some adjustment parameters in the TP algorithm, the obtained climatology contains different types of transient elongated cloud bands connecting the tropics and subtropics. However, they can be further separated by an a priori knowledge of their preferred geographical and seasonal occurrence. Notwithstanding, the new algorithm provides a great opportunity to examine TP climatologies and trends in upcoming homogenized long-term satellite datasets [e.g., Gridded Satellite (GridSat); see Knapp et al. 2011], to compare with alternative approaches based on pattern recognition as in Wick et al. (2013), as well as to conduct more in-depth investigations of the processes discussed in the introduction and section 7, such as moisture and momentum transports (e.g., the relationship to atmospheric rivers), precipitation, and radiation.

REFERENCES

Carvalho, L. M. V., C. Jones, and B. Liebmann, 2004: The South Atlantic convergence zone: Intensity, form, persistence, and relationships with intraseasonal to interannual activity and extreme rainfall. *J. Climate,* **17,** 88–108.

Cook, K. H., 2000: The South Indian Convergence zone and interannual rainfall variability over southern Africa. *J. Climate,* **13,** 3789–3804.

Corti, T., and T. Peter, 2009: A simple model for cloud radiative forcing. *Atmos. Chem. Phys.,* **9,** 5751–5758.

Erickson, C. O., and J. S. Winston, 1972: Tropical storm, mid-latitude, cloud-band connections and the autumnal buildup of the planetary circulation. *J. Appl. Meteor.,* **11,** 23–36.

Evan, A. T., A. K. Heidinger, and D. J. Vimont, 2007: Arguments against a physical long-term trend in global ISCCP cloud amounts. *Geophys. Res. Lett.,* **34,** L04701, doi:10.1029/2006GL028083.

Fink, A. H., and P. Knippertz, 2003: An extreme precipitation event in southern Morocco in spring 2002 and some hydrological implication. *Weather,* **58,** 377–387.

Fröhlich, L., and P. Knippertz, 2008: Identification and global climatology of upper-level troughs at low latitudes. *Meteor. Z.,* **17,** 565–573.

Harrison, E. F., P. Minnis, B. R. Barkstrom, V. Ramanathan, R. D. Cess, and G. G. Gibson, 1990: Seasonal variation of cloud radiative forcing derived from the Earth Radiation Budget Experiment. *J. Geophys. Res.,* **95,** 18 687–18 703.

Hodges, K. I., D. W. Chappell, G. J. Robinson, and G. Yang, 2000: An improved algorithm for generating global window brightness temperatures from multiple satellite infrared imagery. *J. Atmos. Oceanic Technol.,* **17,** 1296–1312.

Hoskins, B. J., and T. Ambrizzi, 1993: Rossby-wave propagation on a realistic longitudinally varying flow. *J. Atmos. Sci.,* **50,** 1661–1671.

Iskenderian, H., 1995: A 10-year climatology of Northern Hemisphere tropical cloud plumes and their composite flow patterns. *J. Climate,* **8,** 1630–1637.

Kiladis, G. N., and K. M. Weickmann, 1992: Circulation anomalies associated with tropical convection during northern winter. *Mon. Wea. Rev.,* **120,** 1900–1923.

——, and ——, 1997: Horizontal structure and seasonality of large-scale circulations associated with submonthly tropical convection. *Mon. Wea. Rev.,* **125,** 1997–2013.

Knapp, K. R., and Coauthors, 2011: Globally gridded satellite observations for climate studies. *Bull. Amer. Meteor. Soc.,* **92,** 893–907.

Knippertz, P., 2005: Tropical-extratropical interactions associated with an Atlantic tropical plume and subtropical jet streak. *Mon. Wea. Rev.,* **133,** 2759–2776.

——, 2007: Tropical–extratropical interactions related to upper-level troughs at low latitudes. *Dyn. Atmos. Oceans,* **43,** 36–62.

——, and J. E. Martin, 2005: Tropical plumes and extreme precipitation in subtropical and tropical West Africa. *Quart. J. Roy. Meteor. Soc.,* **131,** 2337–2365.

——, and ——, 2007: A Pacific moisture conveyor belt and its relationship to a significant precipitation event in the semiarid southwestern United States. *Wea. Forecasting,* **22,** 125–144.

——, and A. H. Fink, 2008: Dry-season precipitation in tropical West Africa and its relation to forcing from the extratropics. *Mon. Wea. Rev.,* **136,** 3579–3596.

——, H. Wernli, and G. Gläser, 2013: A global climatology of tropical moisture exports. *J. Climate,* **26,** 3031–3045.

Kodama, Y.-M., 1992: Large-scale common features of the subtropical precipitation zones (the Baiu frontal zone, the SPCZ, and the SACZ). Part I: Characteristics of subtropical frontal zones. *J. Meteor. Soc. Japan,* **70,** 813–836.

——, 1993: Large-scale common features of the subtropical convergence zones (the Baiu frontal zone, the SPCZ, and the SACZ). Part II: Conditions of the circulations for generating the STCZs. *J. Meteor. Soc. Japan,* **71,** 581–610.

Kuhnel, I., 1989: Tropical-extratropical cloudband climatology based on satellite data. *Int. J. Climatol.,* **9,** 441–463.

McGuirk, J. P., A. H. Thompson, and N. R. Smith, 1987: Moisture bursts over the tropical Pacific Ocean. *Mon. Wea. Rev.,* **115,** 787–798.

——, ——, and J. R. Schaefer, 1988: An eastern Pacific tropical plume. *Mon. Wea. Rev.,* **116,** 2505–2521.

Moore, R. W., O. Martius, and H. C. Davies, 2008: Downstream development and Kona low genesis. *Geophys. Res. Lett.,* **35,** L20814, doi:10.1029/2008GL035502.

Neiman, P. J., F. M. Ralph, G. A. Wick, J. D. Lundquist, and M. D. Dettinger, 2008: Meteorological characteristics and overland precipitation impacts of atmospheric rivers affecting the west coast of North America based on eight years of SSM/I satellite observations. *J. Hydrometeor.,* **9,** 22–47.

Ralph, F. M., P. J. Neiman, and G. A. Wick, 2004: Satellite and CALJET aircraft observations of atmospheric rivers over the eastern North Pacific Ocean during the winter of 1997/98. *Mon. Wea. Rev.,* **132,** 1721–1745.

——, ——, G. N. Kiladis, K. Weickman, and D. W. Reynolds, 2011: A multiscale observational case study of a Pacific atmospheric river exhibiting tropical–extratropical connections and a mesoscale frontal wave. *Mon. Wea. Rev.,* **139,** 1169–1189.

Roberge, A., J. R. Gyakum, and E. H. Atallah, 2009: Analysis of intense poleward water vapor transports into high latitudes of western North America. *Wea. Forecasting,* **24,** 1732–1747.

Schnadt, C., A. Fink, D. G. Vincent, J. M. Schrage, and P. Speth, 1998: Tropical cyclones, 6-25 day oscillations, and tropical-extratropical interaction over the northwestern Pacific. *Meteor. Atmos. Phys.,* **68,** 151–169.

Straus, D. M., and J. Shukla, 2002: Does ENSO force the PNA? *J. Climate,* **15,** 2340–2358.

Thepenier, R.-M., and D. Cruette, 1981: Formation of cloud bands associated with the American subtropical jet stream and their interaction with midlatitude synoptic disturbances reaching Europe. *Mon. Wea. Rev.,* **109,** 2209–2220.

Trenberth, K. E., 1997: The definition of El Niño. *Bull. Amer. Meteor. Soc.,* **78,** 2771–2777.

Uppala, S., and Coauthors, 2005: ERA-40: ECMWF 45-year reanalysis of the global atmosphere and surface conditions 1957-2002. *ECMWF Newsletter,* No. 101, ECMWF, Reading, United Kingdom, 2–21.

Vincent, D. G., 1994: The South Pacific convergence zone (SPCZ): A review. *Mon. Wea. Rev.,* **122,** 1949–1970.

Waugh, D. W., and L. M. Polvani, 2000: Climatology of intrusions into the tropical upper troposphere. *Geophys. Res. Lett.,* **27,** 3857–3860.

Webster, P. J., and J. R. Holton, 1982: Cross-equatorial response to middle-latitude forcing in a zonally varying basic state. *J. Atmos. Sci.,* **39,** 722–733.

Wick, G. A., P. J. Neiman, and F. R. Ralph, 2013: Description and validation of an automated objective technique for identification and characterization of the integrated water vapor signature of atmospheric rivers. *IEEE Trans. Geosci. Remote Sens.,* **51,** 2166–2176.

Yoneyama, K., and D. B. Parsons, 1999: A proposed mechanism for the intrusion of dry air into the tropical western Pacific region. *J. Atmos. Sci.,* **56,** 1524–1546.

Zhu, Y., and R. E. Newell, 1998: A proposed algorithm for moisture fluxes from atmospheric rivers. *Mon. Wea. Rev.,* **126,** 725–735.